From the Hadean to the Himalaya: 4.4 Ga of felsic terrestrial magmatism

T. Mark Harrison[1,*] and Matthew M. Wielicki[1]

[1]Department of Earth, Planetary and Space Sciences, University of California, Los Angles, Los Angeles, California 90095, U.S.A.

Abstract

Detrital zircons as old as nearly 4.4 Ga offer insights into the earliest moments of Earth history. Results of geochemical investigations of these grains have been interpreted to indicate their formation in near-H_2O saturated meta- and peraluminous magmas under a relatively low (15–30 °C/km) geotherm. A key feature in pursuing a petrotectonic model that explains the full spectrum of these observations is their seeming contrast to most Phanerozoic magmatic zircons, specifically their low Ti-in-zircon crystallization temperatures and inclusion assemblages. The ~22 Ma Arunachal leucogranites of the eastern Himalaya appear, however, to be a rare exception to this generality. They show large-ion lithophile covariance trends indicative of wet basement melting together with a normal distribution of magmatic crystallization temperatures about an average of 660 °C. In the same fashion as Hadean zircons, Arunachal leucogranite and host gneiss zircons are dominated by muscovite + quartz inclusions that yield formation pressures of 5–15 kbars. We suggest that the Arunachal leucogranites originated in the hanging wall of a megathrust that carried H_2O-rich foreland sediments to depths of >20 km whereupon de-watering reactions released fluids that fluxed hanging wall anatexis. Modeling suggests the thermal structure of this continental collision environment may have been broadly similar to a Hadean ocean-continent subduction zone. The similarity of these two environments, separated by over 4 Ga may explain seemingly common features of the Hadean and Arunachal leucogranite zircons. Their key difference is the absence of metaluminous magmas in the continental collision environment, which is shielded from juvenile additions.

Keywords: Early Earth, zircon, geochronology, geochemistry, crustal magmas, Himalaya

Introduction

Hadean zircon geochemistry

Much of our understanding of the Hadean—the first 500 Ma of Earth history—is gleaned from detrital zircons as old as nearly 4.4 Ga (see review of Harrison 2009). Hadean zircons, most notably those from Jack Hills, Western Australia, have been analyzed by numerous geochemical methods, including oxygen isotopes (e.g., Mojzsis et al. 2001; Peck et al. 2001; Cavosie et al. 2005; Trail et al. 2007; Harrison et al. 2008; Bell and Harrison 2013), Xe isotopes (Turner et al. 2004, 2007), Ti-in-zircon thermometry (Watson and Harrison 2005; Harrison et al. 2007; Harrison and Schmitt 2007; Fu et al. 2008), Lu-Hf (Amelin et al. 1999; Harrison et al. 2005, 2008; Blichert-Toft and Albarède 2008; Bell et al. 2011, 2013), Sm-Nd (Amelin 2004; Caro et al. 2008), Li isotopes (Ushikubo et al. 2008), trace elements (e.g., Maas and McCulloch 1991; Peck et al. 2001; Cavosie et al. 2005), and characterized for mineral inclusions (Maas et al. 1992; Cavosie et al. 2004; Menneken et al. 2007; Hopkins et al. 2008, 2010, 2012; Rasmussen et al. 2011; Bell et al. 2015).

If any generalization can be drawn from these studies, it is that their results appear inconsistent with the long-standing view that the first several hundred million years of Earth history were characterized by a waterless and molten surface (e.g., Kaula

1979; Wetherill 1980; Solomon 1980; Ward and Brownlee 2000). Alternate views, such as their growth in melts derived from mafic crust (e.g., Rollinson 2008; Shirey et al. 2008), invariably focus on the subset of their geochemical constraints that are consistent with the proposed interpretation while ignoring those that are contradictory (e.g., inclusion assemblages, crystallization temperature). Instead, low (~680 °C) crystallization temperatures, hydrous S- and I-type inclusion assemblages, $\delta^{18}O$ enrichment in some Hadean zircons, and continental trace element signatures indicate melting of crustal protoliths under high-water activities to produce both metaluminous and peraluminous magmas (Harrison 2009). Hopkins et al. (2008, 2010) interpret the relatively low (15–30 °C/km) geotherms obtained from thermobarometry of zircons and their inclusion assemblages to indicate that these magmas formed in plate-boundary-type settings.

Collectively these data suggest that the Hadean world may have been more similar to the present than long thought, raising the question: Is there a modern environment that produces broadly similar geochemical signals?

Himalayan granitoid geochemistry

It is generally agreed that the High-Himalayan leucogranites formed by melting of pelites in the underlying Greater Himalayan Crystallines during Neohimalayan ultrametamorphism (LeFort et al. 1987; Harris and Inger 1992; Guillot and LeFort 1995; LeFort 1996; Harrison et al. 1997; Yin and Harrison 2000; Zhang et al. 2004). However, in the eastern Himalaya, four distinctive modes
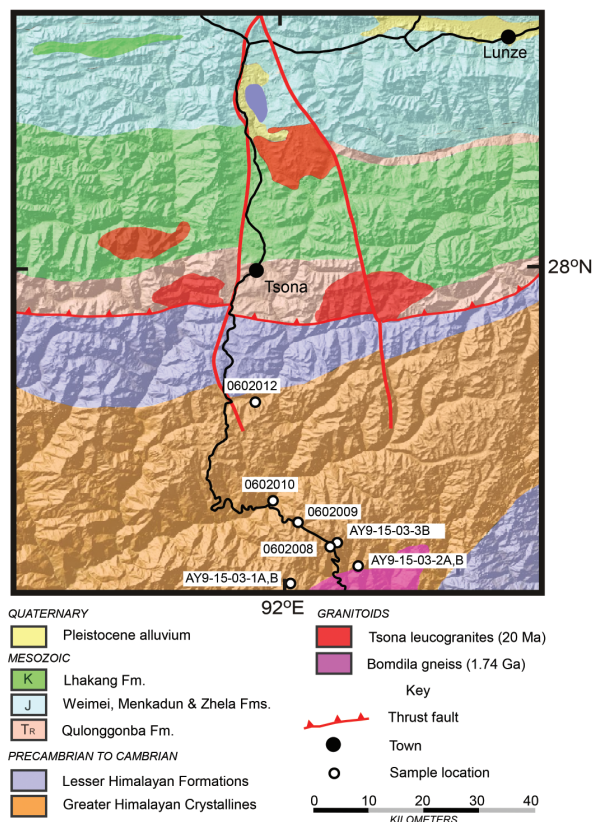
FIGURE 1. Geologic map of the 92° E transect showing sample locations in the sills and dikes of the Arunachal leucogranites and their relationship to the Tsona leucogranites further north. Geology from Pan et al. (2004). (Color online.)

of post-collisional magmatism are evident along a transect at ca. 92°E (Debon et al. 1986; Aikman et al. 2008, 2012a, 2012b; Hou et al. 2012). Two Eocene igneous complexes are emplaced into Tethyan metasediments along the northern portion of the transect, the 44.1 ± 1.2 Ma Dala and 42 ± 5 Ma Yala-Xiangbo granitoids (Aikman et al. 2008, 2012a). The former are interpreted to have formed from sub-equal mixtures of Andean-type magmas and the Greater Himalayan Crystalline basement while the later appear to be evolved equivalents of the Dala suite and contain Miocene reactivation products (Aikman et al. 2012b). Further south, two Miocene intrusive suites (Fig. 1), the Tsona and Arunachal leucogranites, were dated at 18.8 ± 1.2 and 20 ± 2 Ma, respectively, by Aikman et al. (2012a). At first glance they both appear to belong to the aforementioned High Himalayan leucogranite series. The Tsona leucogranites are comprised of pluton-sized bodies (i.e., >10 km^2) and are similar in age and trace element geochemistry to the vast majority of High Himalayan leucogranites (Aikman et al. 2012b). In contrast, the Arunachal leucogranites outcrop as tens-of-meter-scale sills and dikes (Yin et al. 2009) and fall outside the documented range of the large High Himalayan leucogranites in several ways. They exhibit lower $^{87}Rb/^{86}Sr$ and higher $^{87}Sr/^{86}Sr$, and, when coupled with their host rocks, lie along a ~1800 Ma Rb-Sr isochron, which is significantly older than the ca. 500 Ma isochron generally exhibited by the High Himalayan leucogranites

and the Greater Himalayan Crystallines from which they were derived (Aikman et al. 2012b). With few exceptions (e.g., King et al. 2011), the Arunachal leucogranites show a very different character on LILE covariance diagrams to the large Miocene Himalayan leucogranites.

In this paper, we present a range of geochemical results on zircons and their whole rocks from a suite of Arunachal granitoid dikes and sills and zircons from host gneisses and compare these data with the aforementioned database of Hadean zircon analyses. We conclude that special circumstances arising in underthrust environments may have led to development of broadly similar petrotectonic conditions separated in time by over 4.3 billion years.

ANALYTICAL METHODS AND DATA ACQUISITION

Major elements and selected trace elements were determined for five Arunachal ("AY") samples (from the collection of Yin et al. 2009) by X-ray fluorescence at Pomona College using the methodology of Lackey et al. (2012). Samples AY-1A and AY-2A are host gneisses and the other three are undeformed leucogranites. These data and the previously published results from three leucogranites samples analyzed by Aikman et al. (2012a) are given in Table 1.

All U-Pb dating, δ^{18}O, and Ti measurements were undertaken using a CAMECA ims1270 ion microprobe. Samples were mounted in epoxy and polished to reveal a flat surface. We used a primary O⁻ beam intensity of 10–15 nA, corresponding to an analysis spot size of ~25 μm diameter, for U-Pb dating and Ti measurements. U-Pb age standard AS3 (1099 ± 1 Ma; Paces and Miller 1993) was used for the dating studies. Ti measurements, normalized to $^{94}Zr_2O$, were carried out simultaneous with the U-Pb measurements in peak hopping mode. The concentration of Ti was determined based on analysis of standard zircon AS3 (23.4 ppm; Aikman 2007) as well as NIST610 glass. U-Pb and Ti analytical results are given in Table 2.

Oxygen isotope measurements were made in Faraday multicollection mode with a Cs⁺ primary beam intensity of 1–2 nA. The AS3 zircon standard (5.34‰; Trail et al. 2007) was used for sample-standard comparison. For more details on the analytical methods see Trail et al. (2007). δ^{18}O results are given in Table 3.

We surveyed the Arunachal zircon inclusion population (n = 49) and found quartz and muscovite to be by far the most common inclusions making up 63% of the total (39% and 25%, respectively), with 8% K-spar and bio, 4% plag, 2% ap, and 23% multi-mineralic or difficult to distinguish, fine-grained phases. Muscovite inclusions in zircons were chemically analyzed using a JEOL 8600 electron microprobe analyzer (EPMA). Although the EMPA electron beam can be focused to spots as small as ~1 μm, secondary fluorescence effects create a practical limit for the smallest mica dimension to be ≥5 μm in order for Si from the zircon to not contribute to the overall signal. Muscovite EPMA data were normalized to 95% total (i.e., assuming 5% structural H$_2$O) and converted to a formula normalized to 11 O atoms yielding Si per formula unit (Si$_{pfu}$). Volatile loss, monitored via K and Na count rates, appeared to be minor. Summarized data are given in Table 4 and extended results are provided in the supplementary online materials[1].

Electron imagery of all zircons and their inclusions is provided in the supplementary online materials[1] and the image of Arunachal zircon 0602010g2 is reproduced in Figure 4. This grain illustrates the general features of our samples, including the lower crystallization temperature and higher δ^{18}O value in the younger rim (its exact age is uncertain due to a small ion beam rim/core overlap but assumed to be ca. 22 Ma) relative to the Proterozoic core, which exhibits near mantle-like δ^{18}O and a higher crystallization temperature.

RESULTS AND DISCUSSION

Zircon U-Pb geochronology and Ti-thermometry

We undertook spot analyses of zircons from both the Arunachal mount used by Aikman (2007), yielding 40 new U-Pb-Ti age/temperature measurements, and 38 analyses on zircons from the AY samples (Table 1) for a total of 163 age and

temperature determinations. $^{206}Pb/^{238}U$ zircon ages range from 17 to 1076 Ma (Table 1) with pronounced Tertiary and Precambrian age peaks and $^{207}Pb/^{206}Pb$ ages up to 2.4 Ga (Fig. 2). The Tertiary ages are largely neoformed rims, which tail to older ages reflecting the presence of xenocrystic cores. We assumed that the 87 Neogene ages (17–27 Ma), over 50% of the total, reflect neoformed magmatic zircon. This appears a reasonable cutoff as only five Paleogene ages (3% of the total) were documented (Table 1). The Neogene age distribution (Fig. 2a) suggests a bimodal distribution with peaks at ~20 and ~23 Ma and thus the weighted mean age of 22.0 ± 0.6 Ma (2σ) is associated with an MSWD of 60. We interpret this distribution as reflecting a ca. 4 m.y. duration of anatexis and zircon crystallization for the bodies sampled. The distribution of >30 Ma ages (Fig. 2b) is characterized by a series of peaks that correspond to detrital zircon populations known to be present in the Greater Himalayan Crystallines and Tethyan metasediments (Gehrels et al. 2011).

Watson and Harrison (2005) showed that the concentration of Ti in Hadean zircons can be used to estimate crystallization tem-

perature. Although this approach requires an accurate estimate of melt a_{TiO_2} and a_{SiO_2} (Ferry and Watson 2007), the ubiquitous presence of both quartz and rutile in the Arunachal and Tsona leucogranites gives confidence in assuming $a_{TiO_2} \approx a_{SiO_2} \approx 1$. This is less clear for the detrital Hadean zircons, although the common presence of quartz inclusions (Hopkins et al. 2010) generally constrain $a_{SiO_2} \approx 1$ and a_{TiO_2} is likely to be typically ≥0.5 (Watson and Harrison 2005), potentially leading to up to 50 °C temperature underestimates at ca. 680 °C.

Previous zircon analyses from the Arunachal and Tsona leucogranites yielded crystallization temperature peaks with respective averages of 660 and 730 °C (Aikman 2007; Aikman et al. 2012a). The form of the Tsona leucogranite crystallization temperature distribution conforms broadly to simple theory (Harrison et al. 2007) and thus likely records a temperature just below that of peak anatexis. The correspondence of the peak temperature of ~730 °C (Fig. 3) with the inferred position of muscovite breakdown (Douce and Harris 1998), coupled with the LILE covariance evidence, led Aikman et al. (2012b) to

TABLE 1. GPS location and major- and trace-element whole-rock geochemistry for Himalayan grantitoids

Sample	AY-1A	AY-1B	AY-2A	AY-2B	AY-3B	0602008	0602009	0602010	0602012
Latitude	27°25.867′N	27°25.867′N	27°27.526′N	27°27.526′N	27°30.107′N	27°30.107′N	27°32.631′N	27°35.043′N	27°41.083′N
Longitude	92°07.192′E	92°07.192′E	92°08.675′E	92°08.675′E	92°06.268′E	92°06.268′E	92°02.319′E	91°58.325′E	91°46.212′E
SiO_2	75.48	75.33	78.65	74.64	74.75	67.95	74.74	76.01	73.68
TiO_2	0.37	0.10	0.50	0.07	0.06	0.22	0.18	0.10	0.20
Al_2O_3	11.97	14.10	9.96	14.24	14.35	17.00	13.26	15.23	14.03
Fe_2O_3	3.88	1.25	1.69	0.65	0.67	1.67	1.48	1.00	1.96
MnO	0.75	0.01	0.04	0.01	0.01	0.02	0.02	0.01	0.03
MgO	0.48	0.28	0.46	0.09	0.15	0.45	0.37	0.25	0.59
CaO	1.92	1.65	3.26	1.28	1.06	1.18	1.14	1.13	1.28
Na_2O	2.22	3.92	0.72	2.93	3.50	3.80	3.06	3.26	3.48
K_2O	2.72	3.19	4.25	5.92	5.28	6.75	3.99	1.92	3.96
P_2O_5	0.02	0.05	0.22	0.04	0.06	0.09	0.06	0.08	0.11
SUM	99.81	99.88	99.75	99.88	99.90	99.14	98.31	98.99	99.32
Rb	151	169	200	225	223	231.9	142.6	85.8	128.7
Sr	42	77	142	118	69	157.3	90.3	61.4	118.4
Ba	519	196	777	388	338	1002.6	508.9	148.6	556.3
Zr	174	10	344	75	17	112	83.7	46.6	77.3
Y	27	14	41	3	5	30.2	11.1	7.6	25.4
Nb	10	6	13	0	0	8.7	7.1	6.1	8.4
CS	8	6	0	6	12	5.9	7.7	3.3	2.6
Sc	9	3	8	0	3	4.9	5.4	4.9	7.4
V	50	9	34	4	8	68.8	68	69.5	73.3
Cr	171	17	43	16	14	12.9	12	9.1	24.1
Ni	34	0	6	0	0	7.2	7	5.9	5.2
Cu	53	2	15	0	0	2.7	8.7	3	3.5
Zn	46	67	24	6	15	nd	nd	nd	nd
Ga	15	16	12	15	17	16.9	15.3	20.9	14.5
La	23	48	55	13	18	47.7	29.8	13.8	16.4
Ce	113	83	121	19	15	95.7	60.4	27.6	33.8
Pr	4	9	13	0	0	10.8	6.8	3.1	3.9
Nd	30	37	44	7	8	41.8	26.2	11.6	15.4
Sm	nd	nd	nd	nd	nd	10	5.9	3	3.7
Eu	nd	nd	nd	nd	nd	1.8	0.9	0.5	0.7
Gd	nd	nd	nd	nd	nd	10	5.3	2.7	3.9
Tb	nd	nd	nd	nd	nd	1.3	0.6	0.4	0.6
Dy	nd	nd	nd	nd	nd	6.9	2.9	1.9	4.6
Ho	nd	nd	nd	nd	nd	1.1	0.4	0.3	0.9
Er	nd	nd	nd	nd	nd	2.5	1	0.7	2.8
Tm	nd	nd	nd	nd	nd	0.3	0.1	nd	0.5
Yb	nd	nd	nd	nd	nd	1.9	0.8	0.6	3.4
Lu	nd	nd	nd	nd	nd	0.3	0.1	nd	0.5
Hf	3	0	9	4	0	4.4	3.7	2.8	3.5
Pb	94	211	186	155	118	146.3	155.3	60.4	9.7
Th	13	32	24	9	8	35.9	22.5	9.9	9.6
U	0	5	4	0	12	11.2	5.6	4.9	2.6
Mo	nd	nd	nd	nd	nd	0.7	1.3	0.6	0.9
Sn	nd	nd	nd	nd	nd	4	10.8	8.9	1.7
Ta	nd	nd	nd	nd	nd	1.2	1.5	1.5	1.5
Co	nd	nd	nd	nd	nd	37.2	43.1	30.9	30.1

TABLE 2. SIMS U-Pb age data and Ti concentration as well as Ti-in-zircon crystallization temperature

Name	$^{206}Pb/^{238}U$ Age (Ma)	$\pm1\sigma$	$^{207}Pb/^{235}U$ Age (Ma)	$\pm1\sigma$	% Radiogenic ^{206}Pb	$^{206}Pb*/^{238}U$	$\pm1\sigma$	$^{207}Pb*/^{235}U$	$\pm1\sigma$	Correlation of Concordia Ellipses	Ti (ppm)	$\pm1\sigma$	T (°C)	$\pm1\sigma$
0602009g4.2	18.69	1.32	18.3	1.43	99.69	2.90E-3	2.06E-4	1.82E-2	1.44E-3	8.37E-1	5.96	0.60	697	35
0602009g6_2.2	19.08	1.49	19.3	1.73	99.59	2.97E-3	2.32E-4	1.92E-2	1.74E-3	8.62E-1	6.61	0.66	706	35
0602009g7.2	20.14	1.27	20.24	1.47	99.61	3.13E-3	1.97E-4	2.01E-2	1.48E-3	8.77E-1	4.84	0.48	681	34
0602008g21.2	20.31	1.24	18.39	1.61	99.19	3.16E-3	1.93E-4	1.83E-2	1.62E-3	7.16E-1	6.44	0.64	704	35
AY2B.15	21.64	0.343	21.35	1.01	99.52	3.36E-3	5.34E-5	2.13E-2	1.02E-3	4.98E-1	1.92	0.02	614	7
0602010g8.2	21.68	1.67	11.18	9.46	95.19	3.37E-3	2.59E-4	1.11E-2	9.42E-3	3.06E-1	3.13	0.31	648	32
0602009g8.2	21.69	1.48	21.22	1.8	99.68	3.37E-3	2.30E-4	2.11E-2	1.81E-3	7.66E-1	8.54	0.85	727	36
0602010g12.2	21.83	1.5	20.47	1.84	99.52	3.39E-3	2.34E-4	2.04E-2	1.85E-3	7.92E-1	8.04	0.80	722	36
AY2B.10	22.07	0.267	23.29	0.646	99.88	3.43E-3	4.16E-5	2.32E-2	6.51E-4	3.24E-1	2.66	0.03	637	7
AY2B.20	22.43	0.331	22.97	1.17	99.79	3.49E-3	5.16E-5	2.29E-2	1.17E-3	5.30E-1	2.67	0.03	637	7
AY2B.16	22.44	0.308	23.67	1.37	99.66	3.49E-3	4.79E-5	2.36E-2	1.38E-3	2.63E-1	1.68	0.02	605	8
AY2B.7	22.46	0.283	22.89	1.18	99.73	3.49E-3	4.41E-5	2.28E-2	1.19E-3	3.79E-1	4.18	0.04	670	6
AY2B.8	22.79	0.355	23.08	1.12	99.76	3.54E-3	5.52E-5	2.30E-2	1.12E-3	4.34E-1	1.92	0.04	614	13
AY2B.11	22.81	0.59	22.06	0.955	99.59	3.55E-3	9.19E-5	2.20E-2	9.61E-4	1.16E-1	2.81	0.03	640	7
AY2B.21	22.88	0.409	22.63	0.812	99.58	3.56E-3	6.37E-5	2.25E-2	8.18E-4	4.87E-1	2.41	0.04	630	9
0602010g10.2	22.92	1.29	23.11	1.36	99.81	3.56E-3	2.01E-4	2.30E-2	1.37E-3	9.41E-1	6.46	0.65	704	35
AY2B.19	23.03	0.439	23.2	0.739	99.82	3.58E-3	6.83E-5	2.31E-2	7.45E-4	4.16E-1	2.48	0.03	632	7
0602010g11_1.2	23.07	1.35	23.79	1.54	99.33	3.59E-3	2.11E-4	2.37E-2	1.55E-3	8.48E-1	6.54	0.65	705	35
AY2B.9	23.14	0.396	24.23	0.906	99.81	3.60E-3	6.17E-5	2.42E-2	9.14E-4	7.51E-1	2.33	0.03	627	7
AY2B.18	23.15	0.354	23.02	1.33	98.79	3.60E-3	5.52E-5	2.29E-2	1.34E-3	2.79E-1	9.79	1.08	739	41
AY2B.14	23.24	0.687	23.14	1.41	99.61	3.61E-3	1.07E-4	2.31E-2	1.42E-3	5.08E-1	1.74	0.03	607	12
AY2B.3	23.26	0.363	23.56	1.14	99.75	3.61E-3	5.65E-5	2.35E-2	1.15E-3	3.52E-1	2.56	0.03	634	7
AY2B.13	23.27	0.36	25.37	1.77	99.67	3.62E-3	5.60E-5	2.53E-2	1.78E-3	6.22E-1	2.71	0.03	638	7
0602008g2	23.44	1.15	23.59	1.31	99.76	3.64E-3	1.80E-4	2.35E-2	1.32E-3	9.02E-1	4.83	0.48	681	34
AY2B.17	23.47	0.477	23.7	1.22	99.48	3.65E-3	7.43E-5	2.36E-2	1.23E-3	7.26E-1	2.85	0.03	641	8
0602008g22.2	23.59	1.24	23.11	1.85	99.62	3.67E-3	1.94E-4	2.30E-2	1.86E-3	6.98E-1	7.43	0.74	716	36
AY2B.12	23.82	0.302	25.49	1.31	99.24	3.70E-3	4.71E-5	2.54E-2	1.33E-3	4.79E-1	3.76	0.04	662	8
AY2B.1	24.76	0.678	24.42	0.682	99.83	3.85E-3	1.06E-4	2.43E-2	6.88E-4	6.54E-1	2.81	0.03	640	7
AY2B.4	24.99	0.539	24.92	0.703	99.78	3.88E-3	8.39E-5	2.48E-2	7.10E-4	3.59E-1	1.56	0.02	600	8
AY2B.2	25.22	0.673	21.01	1.86	98.2	3.92E-3	1.05E-4	2.09E-2	1.87E-3	3.75E-1	3.92	0.08	665	14
AY2B.5	25.3	0.686	27.36	1.4	99.41	3.93E-3	1.07E-4	2.73E-2	1.42E-3	5.58E-1	7.03	0.12	711	13
AY2B.6	26.44	0.368	27.87	1.06	99.65	4.11E-3	5.74E-5	2.78E-2	1.07E-3	4.71E-1	8.77	0.29	730	12
0602010g13.2	27.25	1.19	27.37	1.33	99.61	4.24E-3	1.85E-4	2.73E-2	1.35E-3	6.69E-1	5.54	0.55	692	35
0602008g7.2	33.84	2.11	36.39	2.25	99.46	5.26E-3	3.29E-4	3.65E-2	2.30E-3	9.15E-1	4.73	0.47	679	34
0602008g8	36.97	1.93	27.09	2.77	97.13	5.75E-3	3.02E-4	2.70E-2	2.80E-3	5.63E-1	13.82	1.42	770	40
0602009g1.2	46.57	1.48	46.96	1.78	99.92	7.25E-3	2.32E-4	4.73E-2	1.84E-3	7.01E-1	6.74	0.34	707	18
0602010g6.1	119.4	6.21	135.9	11.6	99.55	1.87E-2	9.82E-4	1.43E-1	1.30E-2	7.41E-1	5.86	0.59	696	35
0602008g20.2	166	9.9	210.5	11.5	99.93	2.61E-2	1.58E-3	2.30E-1	1.40E-2	9.93E-1	4.44	0.44	674	34
0602008g9	203.3	11.8	226.5	13.8	99.1	3.20E-2	1.88E-3	2.50E-1	1.69E-2	8.89E-1	4.14	0.41	669	33
0602009g1.1	246.6	3.21	292.2	3.24	99.99	3.90E-2	5.17E-4	3.34E-1	4.25E-3	8.93E-1	10.49	0.52	745	19

conclude that the Tsona leucogranites formed via fluid-absent muscovite dehydration melting.

Analyses of neoformed zircons from the Arunachal leucogranites yield a broader distribution than for the Tsona leucogranites, with a dominant peak at ca. 660 °C (Fig. 3; Aikman et al. 2012a; this study). This low temperature, close to that of minimum melting (Luth et al. 1964; Zhang et al. 2004), is consistent with the Arunachal leucogranites forming via fluid-present melting (Aikman et al. 2012a). This crystallization temperature distribution (i.e., a peak at ca. 660 °C) is, to our knowledge, unique (Fig. 3) in documenting growth in granitoid magmas at such low temperatures. While prior reports have yielded similarly low-zircon temperatures (e.g., Fu et al. 2008), such studies have generally failed to systematically assess whether zircon formed under magmatic or sub-solidus conditions by, for example, use of cathodoluminescence imaging and/or establishing the TiO_2 activity during zircon crystallization.

The zircon crystallization temperature spectrum (Fig. 3) that mostly closely resembles the Arunachal leucogranites is that of Hadean igneous zircons (with a peak at ~680 °C) for which a minimum melting origin has also been proposed (see Harrison 2009).

Oxygen isotopes

Oxygen isotope analyses were undertaken on different spots, but wherever possible, within the same CL zone as the U-Pb and Ti analysis spots. Oxygen isotope data gathered on the Arunachal leucogranite zircons are characterized by lighter $\delta^{18}O$ in cores ranging upward from near mantle-like ($\delta^{18}O_{SMOW}$ = 6.0 to 8.0‰; avg. = 6.9‰) to much heavier values in the rims ($\delta^{18}O_{SMOW}$ = 7.4 to 9.8‰; avg. = 8.6‰). Thus the zircon cores are consistent with growth in magmas that had experienced relatively little crustal residence. The heavier $\delta^{18}O$ enrichments in zircons is evidence that the protolith magma from which those zircons formed contained abundant clays (e.g., Mojzsis et al. 2001; Valley 2003).

White mica barometry

In contrast to the claim of Rasmussen et al. (2011) that quartz and white mica inclusions are rare in peraluminous granitoids, we found these phases abundant and in roughly similar proportions in Arunachal leucogranite zircons as that found in the Hadean Jack Hills zircons (Hopkins et al. 2010).

Experimental studies of phengite *P-T* stability (Velde 1965, 1967; Massonne and Schreyer 1987) show that muscovite tends toward the composition of celadonite (i.e., increasing Si^{4+} substitution) with increasing pressure. Thermodynamic properties of white mica based on high-pressure experiments on Al-celadonite end-members (Massonne and Szpurka 1997) allow isopleths of Si content as a function of *P-T* to be calculated within pseudosections for relevant rock compositions (White et al. 2001).

TABLE 2.—CONTINUED

Name	$^{206}Pb/^{238}U$ Age (Ma)	±1σ	$^{207}Pb/^{235}U$ Age (Ma)	±1σ	% Radiogenic ^{206}Pb	$^{206}Pb*/^{238}U$	±1σ	$^{207}Pb*/^{235}U$	±1σ	Correlation of Concordia Ellipses	Ti (ppm)	±1σ	T (°C)	±1σ
AY3A.3	369.4	8.43	382.2	9.46	99.95	5.90E-2	1.39E-3	4.57E-1	1.36E-2	7.69E-1	0.90	0.01	566	9
0602010g12.1	376.7	26.5	408.8	23.2	99.87	6.02E-2	4.35E-3	4.96E-1	3.42E-2	9.49E-1	3.67	0.37	660	33
AY3A.16	389.2	8.3	405.2	7.77	99.92	6.22E-2	1.37E-3	4.90E-1	1.14E-2	8.75E-1	4.64	0.09	678	14
AY3A.15	396.5	64.4	396.4	58.8	99.97	6.34E-2	1.06E-2	4.78E-1	8.55E-2	9.90E-1	1.73	0.26	607	45
AY3A.11	408.2	5.11	418.4	7.2	99.99	6.54E-2	8.44E-4	5.10E-1	1.07E-2	8.83E-1	8.35	0.12	725	10
AY3A.6	436.2	8.19	436.3	6.58	99.92	7.00E-2	1.36E-3	5.37E-1	9.96E-3	2.66E-1	0.36	0.01	514	14
0602010g8.3	448.2	37.5	473.9	36	100	7.20E-2	6.23E-3	5.95E-1	5.66E-2	8.99E-1	3.24	0.32	651	33
AY3A.7	468.5	6.93	478.4	6.05	99.98	7.54E-2	1.16E-3	6.02E-1	9.55E-3	9.23E-1	2.91	0.03	643	7
AY3A.12	489.8	5.99	493.4	4.93	100	7.89E-2	1.00E-3	6.26E-1	7.90E-3	8.44E-1	2.31	0.10	627	14
AY3A.18	491.9	19.3	494.6	15.4	100	7.93E-2	3.24E-3	6.28E-1	2.47E-2	9.89E-1	13.50	0.09	768	5
AY3A.5	496.8	6.33	501.8	5.27	99.98	8.01E-2	1.06E-3	6.39E-1	8.51E-3	9.14E-1	10.80	0.08	748	5
AY3A.14	500.3	8.19	507.6	10	99.98	8.07E-2	1.37E-3	6.49E-1	1.62E-2	9.81E-1	113.03	7.52	1011	34
AY3A.1	510.4	6.76	507.6	6.52	99.98	8.24E-2	1.13E-3	6.49E-1	1.06E-2	5.67E-1	1.90	0.05	613	17
AY3A.2	517.1	7.07	511.1	5.22	99.98	8.35E-2	1.19E-3	6.54E-1	8.50E-3	9.46E-1	2.19	0.03	623	7
AY3A.17	517.6	6.89	517.5	5.89	99.96	8.36E-2	1.17E-3	6.65E-1	9.66E-3	9.51E-1	3.00	0.03	645	7
AY3A.4	522	7.24	520.1	7.12	99.98	8.43E-2	1.22E-3	6.69E-1	1.17E-2	9.49E-1	7.63	0.06	718	6
0602009g5_2.1	522.9	40	997.3	50.9	99.57	8.45E-2	6.74E-3	1.67E+0	1.34E-1	9.97E-1	409.65	61.62	1222	92
AY3A.8	529	6.89	523.5	5.84	99.99	8.55E-2	1.16E-3	6.75E-1	9.64E-3	8.96E-1	3.40	0.04	654	8
AY3A.13	533.8	7	529.9	6.51	99.98	8.63E-2	1.18E-3	6.85E-1	1.08E-2	9.19E-1	5.83	0.07	696	8
AY3A.10	538.7	6.09	531.6	5.65	99.99	8.72E-2	1.03E-3	6.88E-1	9.40E-3	9.54E-1	2.18	0.03	623	7
AY3A.9	562.3	7.24	551.3	5.87	99.99	9.11E-2	1.23E-3	7.21E-1	9.95E-3	9.64E-1	6.29	0.06	702	7
0602009g6_2.1	597.1	45.8	575.4	35.3	99.97	9.71E-2	7.79E-3	7.63E-1	6.12E-2	9.94E-1	1.74	0.17	607	30
0602008g1	621.3	34.9	637.7	28.4	99.89	1.01E-1	5.96E-3	8.74E-1	5.24E-2	9.87E-1	14.17	1.42	773	39
0602009g5.1	633.8	52.6	1149	71.1	99.24	1.03E-1	9.01E-3	2.10E+0	2.17E-1	9.38E-1	213.49	58.35	1107	151
0602008g7.1	656.7	46.3	714.7	39.1	99.9	1.07E-1	7.95E-3	1.02E+0	7.78E-2	9.85E-1	8.75	0.87	729	36
0602008g18	676.9	39.9	663.9	37.2	99.61	1.11E-1	6.88E-3	9.23E-1	7.04E-2	7.97E-1	3.78	0.38	662	33
0602010g2	701.2	11.4	729.8	11.5	100	1.15E-1	1.98E-3	1.05E+0	2.33E-2	7.46E-1	13.47	0.67	768	19
0602008g21.1	710.8	58.7	722.9	43.8	99.92	1.17E-1	1.02E-2	1.04E+0	8.78E-2	9.93E-1	4.13	0.41	669	33
0602008g20.1	735	58.5	755.6	45.1	99.96	1.21E-1	1.02E-2	1.11E+0	9.34E-2	9.98E-1	7.19	0.72	713	36
0602008g22.1	785.3	59.6	800.6	43.8	99.92	1.30E-1	1.04E-2	1.20E+0	9.49E-2	9.89E-1	10.05	1.01	741	37
0602009g8.1	801	57.2	1378	58	99.82	1.32E-1	1.01E-2	2.89E+0	2.22E-1	9.92E-1	19.41	1.94	803	40
0602008g4	821.7	47.3	853.5	34.3	99.93	1.36E-1	8.34E-3	1.32E+0	7.82E-2	9.68E-1	9.73	0.97	739	37
0602008g3.1	853.2	10.7	886.5	9.38	99.99	1.42E-1	1.89E-3	1.39E+0	2.21E-2	9.40E-1	12.99	0.65	764	19
0602008g11	898.6	70.4	881.6	49.9	99.99	1.50E-1	1.26E-2	1.38E+0	1.17E-1	9.97E-1	7.75	0.78	719	36
0602010g10.1	942.3	74.5	949	50.4	99.95	1.57E-1	1.34E-2	1.55E+0	1.26E-1	9.75E-1	14.13	1.41	772	39
0602008g3.2	974.3	12	977.7	8.57	100	1.63E-1	2.17E-3	1.62E+0	2.21E-2	9.10E-1	13.88	0.69	771	19
0602009g7.1	1022	67.8	1071	47.4	99.94	1.72E-1	1.23E-2	1.87E+0	1.34E-1	9.89E-1	10.48	1.05	745	37
0602010g11_1.1	1047	72.5	1027	50.2	99.97	1.76E-1	1.32E-2	1.75E+0	1.36E-1	9.93E-1	3.68	0.37	660	33
0602010g13.1	1076	87.4	1113	60.4	99.92	1.82E-1	1.60E-2	1.99E+0	1.78E-1	9.84E-1	7.17	0.72	712	36
0602009g4.1	1176	571	1130	364	99.81	2.00E-1	1.06E-1	2.04E+0	1.09E+0	1.00E+0	5.36	0.54	962	344

To estimate the pressure of muscovite inclusion entrainment, we used the isopleths calculated by Hopkins et al. (2010) for a peraluminous composition (with temperature taken from the corresponding zircon crystallization temperature) for $Si_{pfu} < 3.25$ and the empirical relationship of Curetti et al. (2008) for ≥3.25. Our five results from Arunachal leucogranite zircons yield a range of Si_{pfu} from 3.06 to 3.18 corresponding to approximate pressures of 5 to 8 kbars (Table 4). We also analyzed two muscovite inclusions from zircons separated from the adjacent basement gneiss (sample 0602005 of Aikman 2007; Table 4), which give Si_{pfu} of 3.22 and 3.45, corresponding to approximate pressures of 10 and 15 kbars, respectively. The highest calculated pressures are exclusively associated with the Precambrian basement sample rather than from the leucogranite zircons, consistent with our general understanding of Neohimalayan metamorphism (LeFort 1996). The total range in pressure (i.e., from 5–15 kbars) is virtually identical to that documented in Hadean zircons (Hopkins et al. 2010). Our purpose here is only to draw attention to the occurrence of muscovite inclusions in continental zircons, the broad range of pressures they record, and their overall similarity to that documented for the Hadean population (Hopkins et al. 2010).

Major and trace element geochemistry

Based on three whole rock samples, Aikman et al. (2012b) concluded that the Arunachal leucogranites are essentially pure

TABLE 3. SIMS $\delta^{18}O$ data and core to rim relationships

Sample	$\delta^{18}O$ (core)	±2σ	Approximate age domain (Ma)	$\delta^{18}O$ (rim)	±2σ	Approximate age domain (Ma)
0602008g1	6.23	0.16	620	8.41	0.16	20
0602008g4	7.10	0.14	820	7.46	0.20	~20
0602008g7	6.98	0.14	650	7.51	0.20	25
0602008g21	7.33	0.13	710	7.47	0.12	23
0602009g1	6.09	0.20	250	9.48	0.17	30
0602009g5	7.80	0.29	630	9.19	0.10	520
0602009g6	6.61	0.14	600	9.43	0.11	20
0602010g2	5.94	0.41	700	9.80	0.20	~20
0602010g6	7.99	0.13	120	8.55	0.13	~20
0602010g8	7.24	0.13	800	8.62	0.14	22
0602010g9	8.63	0.15	NA	9.22	0.13	~20
0602008g11.1	6.96	0.21	900			
0602008g12.1	9.01	0.16	NA			
0602008g18.1	7.57	0.13	680			
0602008g19.1	6.62	0.16	NA			
0602008g3.1	7.69	0.14	850			
0602008g8.1	6.01	0.18	35			
0602008g9.1	5.78	0.19	200			
0602010g4.1	8.70	0.13	NA			
0602010g5.1	8.77	0.16	NA			

melt compositions with little restitic or cumulate feldspar and that intrasample compositional variations reflect only differences in protolith composition, water pressure, and degree of partial melting. Our extended database shows few clear trends in major elements (an exception being decreasing Al with increasing Si) and broadly supports the conclusions of Aikman et al. (2012b).

TABLE 4. EPMA data from mica inclusions including Si_{pfu}

Sample	Age (Ma)	SiO_2	TiO_2	Al_2O_3	MgO	CaO	MnO	ΣFe as FeO	Na_2O	K_2O	Sum	Si_{pfu}
0602005g2	~1200	53.31	1.04	28.28	0.62	0.02	0.01	4.14	0.74	9.48	97.62	3.46
0602005g5	~1800	48.90	1.13	32.82	0.58	0.01	0.00	1.67	0.74	9.91	95.76	3.22
0602008g3	~970	44.83	1.34	32.86	0.93	0.04	0.01	2.97	0.45	10.82	94.25	3.06
0602008g15	~20	42.83	1.46	31.50	1.53	0.03	0.02	4.15	0.52	10.39	92.44	3.01
0602009g1	~245	45.79	0.53	34.61	0.72	0.02	0.00	2.59	0.36	10.84	95.45	3.07
0602009g3	~20	43.68	2.23	21.43	3.02	0.02	0.05	9.64	0.32	10.40	90.78	3.24
0602010g2	~820	46.10	0.29	30.74	0.91	0.00	0.35	4.43	0.37	10.96	94.14	3.18

Fluid-present melting of pelites at 5–10 kbar starts at ~630 °C, whereas under fluid-absent conditions and similar pressures, incongruent muscovite breakdown in typical pelites begins at ca. 740 °C (Douce and Harris 1998). Incongruent fluid-absent biotite melting begins between 760 and 830 °C (Le Breton and Thompson 1988; Koester et al. 2002). Because trace elemental relationships can be uniquely ascribed to each of these melting reactions, selection among them can be made on the basis of composition (e.g., Harris and Inger 1992; Harris et al. 1995; Ayres and Harris 1997), melting temperature (Zhang et al. 2004) or both.

In granitoids, Rb and Sr reside largely in micas and feldspars and thus knowledge of their partition behavior can be used to gain insight into melting reactions. In the case of fluid-present melting, Harris and Inger (1992) argued that since restite is depleted in feldspar (i.e., the principal host of Sr and Ba), the corresponding liquid should be characterized by low-Rb/Sr and high-Sr/Ba ratios. Fluid-absent melting of muscovite (i.e., the principal host of Rb) reduces the amount of muscovite and increases the proportion of feldspar in the restite resulting in a liquid characterized by a high-Rb/Sr ratio (Harris and Inger 1992). Incongruent, fluid-absent melting of both muscovite and biotite (i.e., a mica-free restite) is expected to lead to even stronger Rb enrichment.

Figures 5a and 5b are plots of Rb/Sr vs. Sr and Ba, respectively (Aikman et al. 2012a; this study; Table 1), showing data
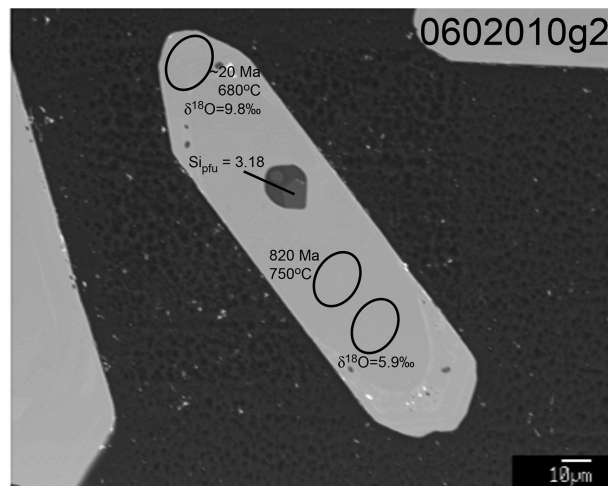
FIGURE 4. Electron micrograph of Arunachal zircon 0602010g2. Note the core/rim relationship with the younger rim exhibit the lower crystallization temperature and higher $\delta^{18}O$ value compared with the older, higher temperature and isotopically lighter core. The muscovite inclusion exhibits a quasi-hexagonal crustal habit and coexists with feldspar. The elliptical feature in the feldspar marks the EMPA spot.
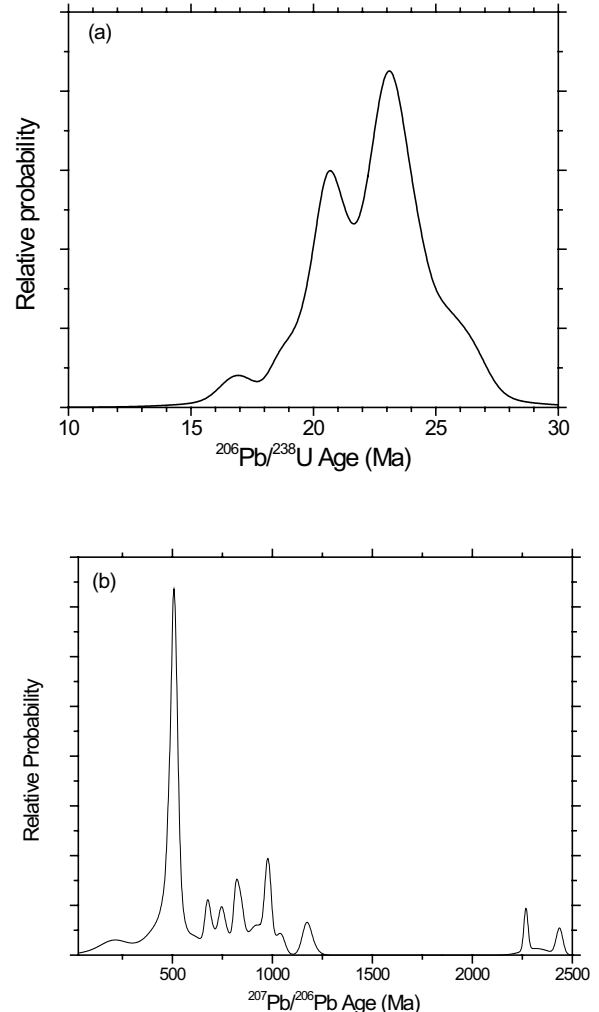
FIGURE 2. (**a**) Probability density function of <30 Ma $^{206}Pb/^{238}U$ zircon ages from the Arunachal leucogranite suite. (**b**) Probability density function of >30 Ma $^{207}Pb/^{206}Pb$ zircons from the Arunachal leucogranite suite. Note the different enlarged scale of relative probability of **b** compared to **a**.

from three large High Himalayan leucogranite plutons (Manalsu, Badrinath-Gangotri, Bhutan), averages of Greater Himalayan Crystalline gneisses (open stars, Colchen et al. 1986 and Harris and Inger 1992; gray stars, Vidal et al. 1982), and the two host gneisses (black stars; AY01A and AY-2A; Table 1). Covariance vectors for the three abovementioned melting reactions (from Inger and Harris 1993) are also shown. It is clear in both plots that the large leucogranites plot parallel to the muscovite vapor
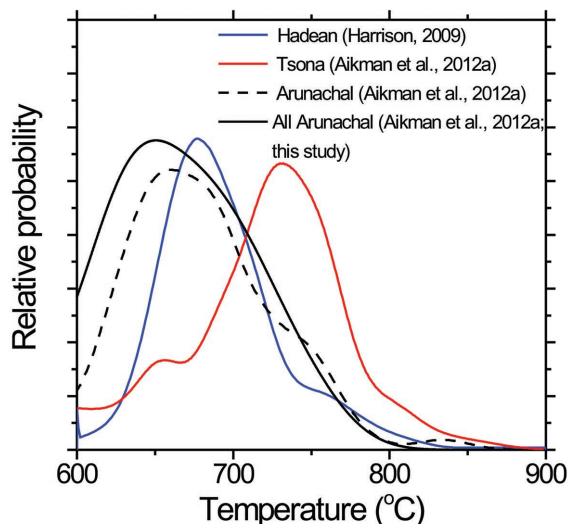
FIGURE 3. Relative probability plot of zircon crystallization temperatures for Himalayan leucogranites from the 92°E transect in eastern Himalaya relative to the Hadean zircon population. (Color online.)

absent vectors while Arunachal leucogranites cluster close or adjacent to the GHC source rocks (gray field in Figs. 5a and 5b), supporting the role of wet melting in their generation.

A possible ambiguity in both these diagrams is that K-feldspar fractionation trends parallel the muscovite vapor absent melting vector. However, petrographic observations indicate K-feldspar was a late crystallizing phase and thus the trends seen in Figures 5a and 5b are unlikely to be due to fractionation. Indeed, separation of cumulate K-feldspar is generally thought not to be generally significant in Himalayan leucogranites (e.g., Inger and Harris 1993).

The clear trend of the large High Himalayan leucogranites parallel to the muscovite fluid-absent melting vector seriously challenged the long-standing paradigm of wet-melting due to the influx of fluids derived from the dehydration of lower plate rocks (the "hot iron" model; LeFort 1975; LeFort et al. 1987; England et al. 1992). It is now widely accepted that the large High Himalayan leucogranites formed by fluid-absent melting of mica-schists in the underlying Greater Himalayan Crystalline (Harris and Inger 1992; Inger and Harris 1993; Harrison et al. 1999; Zhang et al. 2004). Nonetheless, volumetrically minor fluid-present melts, such as the anastamosing, equigranular granites (AEG) of King et al. (2011), indicate that water-saturated melting occurred locally during the early Miocene. Geochemical results for the AEG are also shown in Figures 5a and 5b, as expected, plot close to the gray fields, which define the basement GHC source rocks.

While the Tsona leucogranites follow the fluid-absent melting trend of the large Himlaayan plutons yield an average Rb/Sr of 8 (ranging up to 30), the average Rb/Sr of the Arunachal leucogranites is ~2 and plots within or adjacent the fields of Greater Himalayan crystallines source rocks with an average Rb/Sr of ~1.3 (Vidal et al. 1982; Colchen et al. 1986; Harris and Inger 1992). The lack of strong enrichment in Rb/Sr indicates that the Arunachal leucogranites formed by a process that more equally consumed feldspar, quartz, and mica than would muscovite dehydration melting. Coupled with the low-crystallization temperatures, these data indicate that fluid-present melting was an important contributor to formation of the Arunachal leucogranites (Fig. 5).

Last, the experiments of Douce and Harris (1998) showed that mica dehydration melting leads to normative feldspar compositions that are restricted to within the granite field (Barker 1979), whereas H_2O-fluxed melting yields compositions ranging from granite into the trondhjemite field. The Arunachal leucogranites samples (AY-1B and 602010) show just this distribution with
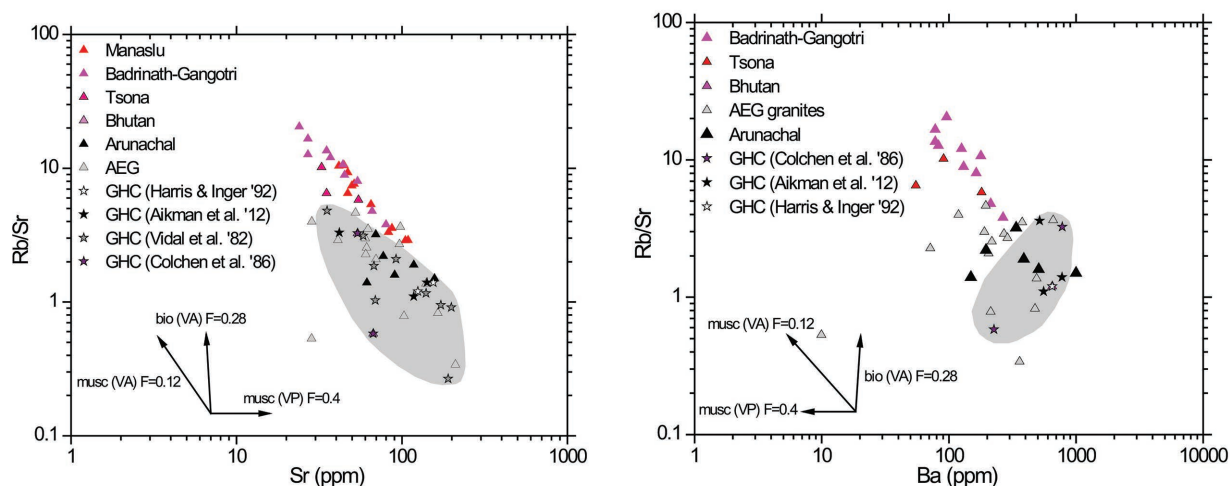

FIGURE 5. Rb/Sr vs. Sr plot (**left**) and Rb/Sr vs. Ba plot (**right**) for Himalayan leucogranites (in warm colors), the Arunachal leucogranites (black circles), averages for the Greater Himalayan Crystallines (open stars), the two host orthogniesses from this study (filled stars), and the field of GHC gneisses from the study of Vidal et al. (1982) in gray (one anomalously low-Rb/Sr datum is omitted). Note that the covariance vector expected for muscovite vapor absent melting (musc VA) is parallel to the trend exhibited by all Himalayan leucogranites except Arunachal, which falls between that array and the trend for basement rocks but within the variance shown in gray. The fraction of melting used in the vector calculation is given by F. (Color online.)

two of the six plotting in the trondhjemitic field and the rest in the granite field (Table 1). This broad range is consistent with the above conclusion that fluid-present melting was important in the formation of the Arunachal leucogranites.

Source of water for anatexis

While it is now widely accepted that the High Himalayan leucogranites formed dominantly by vapor-absent melting of the underlying Greater Himalayan Crystallines during Neohimalayan metamorphism (e.g., Harris and Inger 1992; Zhang et al. 2004), from the mid-1970s to early-1990s their origin was widely ascribed to the "hot iron" model (LeFort 1975; England et al. 1992). In this concept, slip on the Main Central Thrust brought the hot Greater Himalayan Crystallines hanging wall from great depth, juxtaposing this slab against the cooler footwall comprised of the Lesser Himalayan Sequences (LeFort 1975). Lateral heat flow across the Main Central Thrust was hypothesized as the driver of footwall dehydration, with the released fluids fluxing into the still hot hanging wall and causing anatexis of the Greater Himalayan Crystallines. This appeared to explain both the formation of the High Himalayan leucogranites and the apparent increase in metamorphic grade up section toward Main Central Thrust—the classic Himalayan inverted metamorphic sequence (e.g., England et al. 1992). Serious problems with this model began to emerge in the early 1990s. The recognition that the High Himalayan leucogranites did not form by H_2O-saturated melting (Harris and Inger 1992) fueled skepticism that the enormous flow stresses required to generate the needed frictional heating (England and Molnar 1993) could be sustained during continental thrusting. Subsequently, it was discovered that Greater Himalayan Crystalline anatexis and apparent inverted metamorphism in the footwall are not temporally related (Harrison et al. 1997), with footwall recrystallization occurring during the Late Miocene/Pliocene.

The Siang window is a significant structural reentrant in the eastern Himalayan arc directly south of the Namche Barwa syntaxis (Yin et al. 2009). It is defined by a closed trace of the Main Boundary Thrust that places the Lesser Himalayan Sequence over Cretaceous-Paleogene strata (Kumar 1997). As a result, regional structural features, including the Main Central Thrust and Indus-Tsangpo Suture, all make sharp bends around the window. Yin et al. (2009) extrapolated the exposure of the Cretaceous-Paleogene molasse (as far north as 29.3°N) along-strike to the southwest (cross section shown in Fig. 6). In their reconstructed cross-section along the join *I-I′*, ~200 km to the southwest of the Siang window, the Cretaceous-Paleogene molasse today sit beneath the along-strike extrapolation of the Arunachal leucogranites source (Fig. 6). If this were the structural relationship during the early Miocene, then permeable and potentially water-bearing, first-generation coarse clastic sediments were directly beneath the present position of the Arunachal leucogranites. Such a relationship appears to be distinctly different from leucogranite sources elsewhere in the Himalaya, which are interpreted to be largely underlain by the Lesser Himalayan metasediments. Because the Lesser Himalayan Sequence experienced dehydration during both Pan African and Eohimalayan metamorphisms (LeFort 1996), they are unlikely to have been a significant source of fluid with which to catalyze Neogene melting (thus explaining the broadly vapor absent

nature of Himalayan magmatism). However, we believe that the "hot iron" model (LeFort 1975) may be valid for the perhaps unique case of the Arunachal leucogranites, which formed in the hanging wall of a megathrust that carried hydrous sediments to greater than 20 km depths thereupon liberating H_2O, which fluxed across the Main Central thrust to drive anatexis.

Thermal structure

To summarize, Arunachal zircons (both core and rims) yield a *P-T* range (660 to 750 °C and 5 to 15 kbars) that is remarkably similar to that seen in the Jack Hills Hadean zircon population (this study; Hopkins et al. 2010). The similarity of zircon formation separated by over 4 Ga could indicate broadly comparable settings in which footwall dewatering drove hanging wall anatexis (although we note that the highest pressure Arunachal inclusion assemblages are pre-collisional).

Hopkins et al. (2010) undertook a thermal simulation constrained by the heat flow scaling relationship of Korenaga (2006) in which high degrees of mantle melting (due to high-Hadean interior temperatures) lead to sluggish convection resulting in secular heating of the Archean-Hadean mantle. For a mantle potential temperature of 1600 °C and Urey ratio of 0.15 at 4 Ga, Korenaga (2006) calculated that a ~140 km thick oceanic lithosphere would become neutrally buoyant in about 120 Ma, implying an average plate velocity of ~2 cm/yr. Using that footwall thermal structure underthrusting a "continental lithosphere" of 50 km thickness, Hopkins et al. (2010) calculated hanging wall temperatures between 650 to 750 °C at pressures from 6 to ~15 kbar. While their model was highly simplified (e.g., no counter flow in the upper plate), the 650 to 750 °C temperatures persist across depths from 20 to 50 km (i.e., corresponding to the 5 to 15 kbar pressure range observed from the barometric studies). Given depths as shallow as 20 km, they argued that dehydration reactions compressed into a narrow depth region could enhance hydrofracturing and the transport of abundant, water-rich fluids to the site of melting.

The Indo-Asian collision has been the focus of numerous thermal modeling studies over nearly four decades that have investigated the effects of delamination, contrasting thermal conductivities, lower plate accretion, varying ramp-flat geometry, out-of-sequence thrusting, and duplex formation (e.g., Bird 1978; Jaupart 1983; Ruppel and Hodges 1994; Henry et al. 1997; Harrison et al. 1997, 1998; Huerta et al. 1998; Bollinger et al. 2004; Célérier et al. 2009). Increasingly, petrological and thermochronological evidence support the view that, since the mid-Miocene, the Himalayan range grew by underplating due to the southward migration of a midcrustal ramp (Bollinger et al. 2004). Thus the apparent inverted metamorphic sequence results from duplexing and post-metamorphic shearing rather than by relaxation of the saw-tooth geotherm predicted by the "hot iron" model (e.g., England et al. 1992). An example of such a simulation from the study of Célérier et al. (2009), assuming overthrusting of 5 mm/yr under a total convergence rate of 20 mm/yr, is shown in Figure 7. The hanging wall region corresponding to 650 to 750 °C and 6 to 15 kbars (i.e., that broadly observed in both the Hadean and Arunachal zircons) is outlined in white. This broad thermal structure may well be characteristic of Phanerozoic/Proterozoic margins and thus the full range of pressures and temperatures documented in the neoformed and
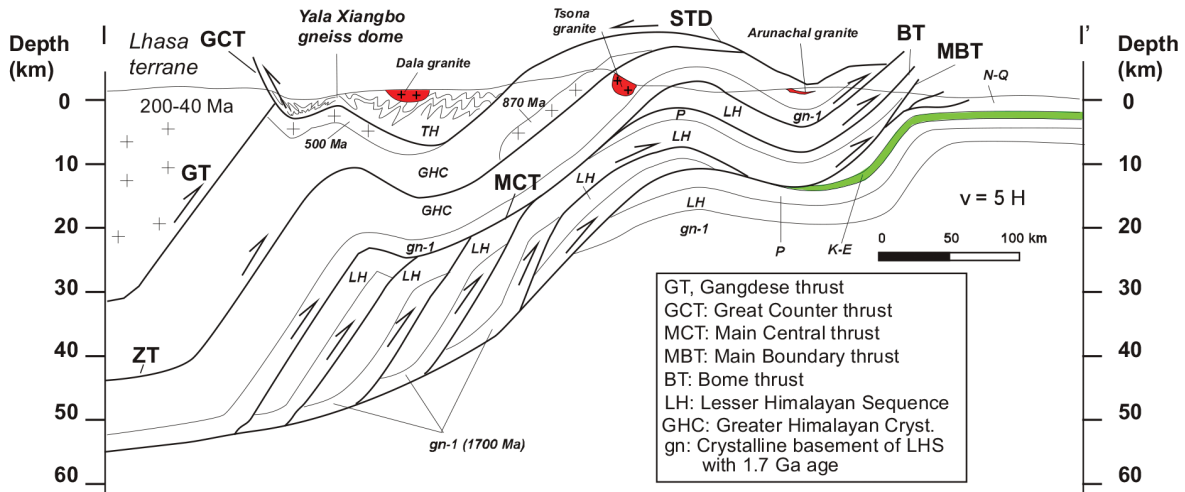
FIGURE 6. Cross-section reconstruction of the eastern Himalaya along 92°E transect, ~200 km SW of the Siang window. This places Cretaceous-Paleogene molasse mapped in the window structurally beneath the present day position of the Arunachal leucogranites. Modified from Yin et al. (2009). (Color online.)

inherited zircons of the Arunachal leucogranites are consistent with their origin in continent-continent collisions.

We appreciate that the approach of Korenaga (2006) is controversial and that thermal modeling of Hadean Earth is underconstrained and in its infancy. Our point is only that it is physically plausible that the thermal structure of a Hadean continental arc and modern continent-continent collision could be broadly similar and that the shared attributes of the Arunachal and >4 Ga zircons could reflect the generation of felsic magmas under not only similar *P-T* and heat flow conditions, but also geologic setting. A key difference is the absence of mantle-derived magmas in the Himalaya, which reflect the intracontinental collision setting. In contrast, Hadean underthrusting in a convergent margin setting could have brought a co-equal mixture of continental-derived sediment and oceanic crust to the melting zone, producing both S- and I-type magmas directly from the interface between subducting sediment and mantle wedge. Such

an environment explains virtually all the myriad characteristics winnowed thus far from these ancient grains.

IMPLICATIONS

Earliest Earth is one of the last great frontiers for fundamental discovery in the geosciences (DePaolo et al. 2008). However, the lack of a rock record older than 4 Ga (Bowring and Williams 1999; cf. O'Neil et al. 2008) potentially leaves only a few strategies with which to investigate the geophysical conditions—and thus habitability—of this most formative phase of our planet's history. Some argue that the fragmentary lithic record that detrital Hadean zircons represent may never permit "smoking gun" conclusions to be drawn about earliest Earth due to its biased nature (e.g., the 70% of the Earth's surface that is today covered by MORB contributes essentially nothing to the detrital zircon archive). In philosophical contrast, geodynamic modelers are beginning to approach the question of earliest Earth from
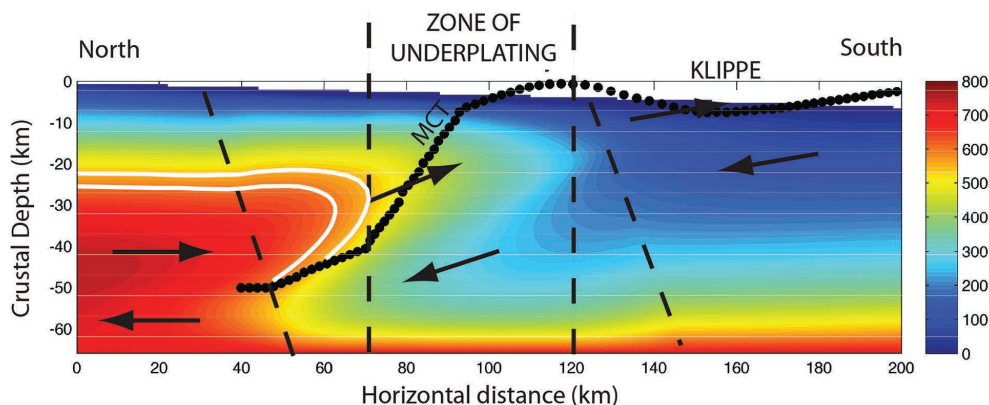
FIGURE 7. Results of a thermo-kinematic simulation of the late Tertiary evolution of the Himalaya after 35 Ma of coupled underplating and surface exhumation. The black dots mark the position of the modeled Main Central thrust (MCT)—the boundary between oppositely verging units. The black arrows show the relative velocity field on either side of the MCT. The region outlined in white corresponds to the pressure-temperature range of 650 to 750 °C and 6 to 18 kbars documented in both Arunachal and Hadean zircons. Modified from Célérier et al. (2009). (Color online.)

perspectives that range from viewing lithic evidence as a potential distraction to discovery of radically new physical scaling relationships (e.g., Sizova et al. 2010), to selective use of those constraints (Marchi et al. 2014), to an approach that balances the limitations of the detrital record with tenable assumptions regarding Hadean dynamics (O'Neill and Debaille 2014). Our view is that documenting comparators of the Hadean zircons in the modern record permits tests of their implications in concrete geologic scenarios that could help reconcile the nascent schism between observation and modeling.

CONCLUDING REMARKS

Geochemical investigations of Hadean zircons suggest their formation in near-H_2O saturated meta- and peraluminous magmas at ca. 680 °C. In contrast, virtually all Himalayan leucogranites investigated show evidence of having been generated under vapor absent conditions at ca. 730 °C. However, the ~22 Ma Arunachal leucogranites, eastern Himalaya, appear to be an exception. They do not show the LILE covariance trend of Himalayan leucogranites but instead show a relationship indicative of wet basement melting and yield a normal distribution of magmatic zircon crystallization temperatures about an average of 660 °C. In the same fashion as Hadean zircons, Arunachal zircon rims and inherited cores are dominated by an inclusion assemblage of muscovite + quartz and yield a range of formation pressures from 5–15 kbars with the higher values recorded in a basement sample. The seemingly unique character of the Arunachal leucogranites within the Himalayan setting suggests an origin that may have aspects in common with the Hadean zircon population. We infer that the Arunachal leucogranites formed in the hanging wall of a megathrust that quickly carried first cycle, water-bearing, clastic sediments to depths of >20 km. When released, this water then ascended into the hanging wall to flux anatexis. Thermal simulations indicate that the heat flow budget of a modern continental collision could be similar to that of a model Hadean ocean-continent subduction margin.

The geochemical similarities between the Hadean and Arunachal leucogranites zircon population—separated in their formation by over 4 Ga—is consistent with comparable geologic settings for their origins. A key difference is the complete absence of mantle-derived, metaluminous magmas in the Himalayan case, reflecting the penetration barrier introduced by doubly thickened continental crust. In contrast, Hadean underthrusting may have brought a co-equal mixture of continental-derived sediment and oceanic crust to the melting zone, producing both S- and I-type magmas directly from the interface between subducting sediment and mantle wedge.

We have previously argued that the Hadean zircon population reveals evidence of water-saturated anatexis occurring during underthrusting in a ~25 °C/km geotherm, which formed peraluminous magmas, some of which were enriched in $\delta^{18}O$. In this paper, we find that the Miocene Arunachal leucogranites formed by mechanisms including water-saturated anatexis during underthrusting in a ~25 °C/km geotherm, which formed peraluminous magmas, including those enriched in $\delta^{18}O$. While much has surely changed on our planet over the past 4.4 billion years, there may be more similarities to these two phases of Earth history than previously thought.

REFERENCES CITED

Aikman, A.B. (2007) Tectonics of the Eastern Tethyan Himalaya. Ph.D. thesis, Research School of Earth Sciences, The Australian National University.

Aikman, A.B., Harrison, T.M., and Lin, D. (2008) Evidence for early (>44 Ma) crustal thickening, Tethyan Hiamalaya, southeastern Tibet. Earth and Planetary Science Letters, 274, 14–23.

Aikman, A.B., Harrison, T.M., and Herman, J. (2012a) Age and thermal history of Eo- and Neohimalayan granitoids, Eastern Himalaya. Journal of Asian Earth Sciences, 51, 85–97.

——— (2012b) The origin of Eo- and Neohimalayan granitoids, Eastern Tibet. Journal of Asian Earth Sciences, 58, 143–157.

Amelin, Y. (2004) Sm-Nd systematics of zircon. Chemical Geology, 211, 375–387.

Amelin, Y.V., Lee, D.C., Halliday, A.N., and Pidgeon, R.T. (1999) Nature of the Earth's earliest crust from hafnium isotopes in single detrital zircons. Nature, 399, 252–255.

Ayres, M., and Harris, N. (1997) REE fractionation and Nd-isotope disequilibrium during crustal anatexis: Constraints from Himalayan leucogranites. Chemical Geology, 139, 249–269.

Barker, F. (1979) Trondhjemite: Definition, environment and hypotheses of origin. In F. Barker, Ed., Trondhjemites, Dacites, and Related Rocks, 6, p. 1–12. Elsevier, Amsterdam.

Bell, E.A., and Harrison, T.M. (2013) Post-Hadean transitions in Jack Hills zircon provenance: A signal of the Late Heavy Bombardment? Earth and Planetary Science Letters, 364, 1–11.

Bell, E.A., Harrison, T.M., McCulloch, M.T., and Young, E.D. (2011) Early Archean crustal evolution of the Narryer Gneiss Complex inferred from Lu-Hf systematics of Jack Hills zircons. Geochimica et Cosmochimica Acta, 75, 4816–4829.

Bell, E.A., Boehnke, P., Hopkins-Wielicki, M.D., and Harrison, T.M. (2015) Distinguishing primary and secondary inclusion assemblages in Jack Hills zircons. Lithos, 234, 15–26.

Bird, P. (1978) Initiation of intracontinental subduction in the Himalaya. Journal of Geophysical Research, 83, 4975–4987.

Blichert-Toft, J., and Albarède, F. (2008) Hafnium isotopes in Jack Hills zircons and the formation of the Hadean crust. Earth and Planetary Science Letters, 265, 686–702.

Bollinger, L., Avouac, J.P., Beyssac, O., Catlos, E.J., Harrison, T.M., Grove, M., Goffé, B., and Sapkota, S. (2004) Thermal structure and exhumation history of the Lesser Himalaya in central Nepal. Tectonics, 23, TC5015.

Bowring, S.A., and Williams, I.S. (1999) Priscoan (4.00-4.03 Ga) orthogneisses from northwestern Canada. Contributions to Mineralogy and Petrology, 134, 3–16.

Caro, G., Bennett, V.C., Bourdon, B., Harrison, T.M., Mojzsis, S.J., and Harris, J.W. (2008) Precise analysis of $^{142}Nd/^{144}Nd$ in small samples: Application to Hadean zircons from Jack Hills (W. Australia) and diamond inclusions from Finsch (S. Africa). Chemical Geology, 247, 253–265.

Cavosie, A.J., Wilde, S.A., Liu, D., Weiblen, P.W., and Valley, J.W. (2004) Internal zoning and U-Th-Pb chemistry of Jack Hills detrital zircons: a mineral record of early Archean to Mesoproterozoic (4348–1576 Ma) magmatism. Precambrian Research, 135, 251–279.

Cavosie, A.J., Valley, J.W., Wilde, S.A., and EIMF (2005) Magmatic $\delta^{18}O$ in 4400–3900 Ma detrital zircons: A record of the alteration and recycling of crust in the Early Archean. Earth and Planetary Science Letters, 235, 663–681.

Célérier, J., Harrison, T.M., Beyssac, O., Herman, F., Dunlap, W.J., and Webb, A.A.G. (2009) The Kumaun and Garwhal Lesser Himalaya, India. Part 2: Thermal and deformation histories. Geological Society of America Bulletin, 121, 1281–1297.

Colchen, M., LeFort, P., and Pêcher, A. (1986) Recherches géologiques dans l'Himalaya du Népal Annapurna, Manaslu, Ganesh: Paris, Editions du Centre National de la Recherche Scientifique, Paris, 136 p.

Curetti, N., Ferraris, G., and Ivaldi, G. (2008) Correlation between crystallization pressure and structural parameters of phengites. American Mineralogist, 93, 451–455.

Debon, F., LeFort, P., Sheppard, S., and Sonet, J. (1986) The four plutonic belts of the Transhimalaya-Himalaya: A chemical, mineralogical, isotopic, and chronological synthesis along a Tibet-Nepal granite section. Journal of Petrology, 27, 219–250.

DePaolo, D.J., Cerling, T.E., Hemming, S.R., Knoll, A.H., Richter, F.M., Royden, L.H., Rudnick, R.L., Stixrude, L., and Trefil, J.S. (2008) Origin and Evolution of Earth: Research questions for a changing planet, 152 pp. National Academy Press, Washington, D.C.

Douce, A.E.P., and Harris, N.B.W. (1998) Experimental constraints on Himalayan anatexis. Journal of Petrology, 39, 689–710.

England, P., and Molnar, P. (1993) The interpretation of inverted metamorphic isograds using simple physical calculations. Tectonics, 12, 145–157.

England, P., LeFort, P., Molnar, P., and Pecher, A. (1992) Heat sources for Tertiary magmatism and anatexis in the Annapurna-Manaslu region of Central Nepal. Journal of Geophysical Research, 97, 2107–2128.

Ferry, J.B., and Watson, E.B. (2007) New thermodynamic models and revised calibrations for the Ti-in-zircon and Zr-in-rutile thermometers. Contributions to Mineralogy and Petrology, 154, 429–437.

Fu, B., Page, F.Z., Cavosie, A.J., Fournelle, J., Kita, N.T., Lackey, J.S., Wilde, S.A., and Valley, J.W. (2008) Ti-in-zircon thermometry: Applications and limitations. Contributions to Mineralogy and Petrology, 156, 197–215.

Gehrels, G., Kapp, P., DeCelles, P., Pullen, A., Blakey, R., Weislogel, A., Lin, D., Guynn, J., Martin, A., McQuarie, N., and Yin, A. (2011) Detrital zircon geochronology of pre-Tertiary strata in the Tibetan-Himalayan orogen. Tectonics, 30, TC5016.

Guillot, S., and LeFort, P. (1995) Geochemical constraints on the bimodal origin of High Himalayan leucogranites. Lithos, 35, 221–234.

Harris, N., and Inger, S. (1992) Trace element modelling of pelite-derived granites. Contributions to Mineralogy and Petrology, 110, 46–56.

Harris, N., Ayres, M., and Massey, J. (1995) Geochemistry of granitic melts produced during the incongruent melting of muscovite—Implications for the extraction of Himalayan leukogranite magmas. Journal of Geophysical Research, 100, 15767–15777.

Harrison, T.M. (2009) The Hadean crust: Evidence from >4 Ga zircons. Annual Reviews of Earth and Planetary Science, 37, 479–505.

Harrison, T.M., and Schmitt, A.K. (2007) High sensitivity mapping of Ti distributions in Hadean zircons. Earth and Planetary Science Letters, 261, 9–19.

Harrison, T.M., Lovera, O.M., and Grove, M. (1997) New insights into the origin of two contrasting Himalayan granite belts. Geology, 25, 899–902.

Harrison, T.M., Grove, M., Lovera, O.M., and Catlos, E.J. (1998) A model for the origin of Himalayan anatexis and inverted metamorphism. Journal of Geophysical Research, 103, 27017–27032.

Harrison, T.M., Grove, M., McKeegan, K.D., Coath, C.D., Lovera, O.M., and LeFort, P.L. (1999) Origin and episodic emplacement of the Manaslu intrusive complex, central Himalaya. Journal of Petrology, 40, 3–19.

Harrison, T.M., Blichert-Toft, J., Müller, W., Albarede, F., Holden, P., and Mojzsis, S.J. (2005) Heterogeneous Hadean hafnium: Evidence of continental crust by 4.4–4.5 Ga. Science, 310, 1947–1950.

Harrison, T.M., Watson, E.B., and Aikman, A.B. (2007) Temperature spectra of zircon crystallization in plutonic rocks. Geology, 35, 635–638.

Harrison, T.M., Schmitt, A.K., McCulloch, M.T., and Lovera, O.M. (2008) Early (≥4.5 Ga) formation of terrestrial crust: Lu-Hf, δ18O, and Ti thermometry results for Hadean zircons. Earth and Planetary Science Letters, 268, 476–486.

Henry, P., LePichon, X., and Goffe, B. (1997) Kinematic, thermal and petrological model of the Himalayas: Constraints related to metamorphism within the underthrust Indian crust and topographic elevation. Tectonophysics, 273, 31–56.

Hopkins, M., Harrison, T.M., and Manning, C.E. (2008) Low heat flow inferred from >4 Gyr zircons suggests Hadean plate boundary interactions. Nature, 456, 493–496.

——— (2010) Constraints on Hadean geodynamics from mineral inclusions in >4 Ga zircons. Earth and Planetary Science Letters, 298, 367–376.

——— (2012) Metamorphic replacement of mineral inclusions in detrital zircon from Jack Hills, Australia: Implications for the Hadean Earth: Comment. Geology, 40, 281–281.

Hou, Z.Q., Zheng, Y.C., Zeng, L.S., Gao, L.E., Huang, K.X., Li, W., and Sun, Q.Z. (2012) Eocene–Oligocene granitoids in southern Tibet. Constraints on crustal anatexis and tectonic evolution of the Himalayan orogen. Earth and Planetary Science Letters, 349, 38–52.

Huerta, A.D., Royden, L.H., and Hodges, K.V. (1998) The thermal structure of collisional orogens as a response to accretion, erosion, and radiogenic heating. Journal of Geophysical Research, 103, 15287–15302.

Inger, S., and Harris, N. (1993) Geochemical constraints on leucogranite magmatism in the Langtang Valley, Nepal Himalaya. Journal of Petrology, 34, 345–368.

Jaupart, C. (1983) Horizontal heat transfer due to radioactivity contrasts: Causes and consequences of the linear heat flow relation. Geophysical Journal International, 75, 411–435.

Kaula, W.M. (1979) Thermal evolution of Earth and Moon growing by planetesimal impacts. Journal of Geophysical Research: Solid Earth, 84, 999–1008.

King, J., Harris, N., Argles, T., Parrish, R., and Zhang, H. (2011) Contribution of crustal anatexis to the tectonic evolution of Indian crust beneath southern Tibet. Geological Society of America Bulletin, 123, 218–239.

Koester, E., Pawley, A.R., Luis, A.D., Fernandes, L.A.D., Porcher, C.C., and Soliani, E. (2002) Experimental melting of cordierite gneiss and the petrogenesis of syntranscurrent peraluminous granites in southern Brazil. Journal of Petrology, 43, 1595–1616.

Korenaga, J. (2006) Archean geodynamics and the thermal evolution of Earth. Archean Geodynamics and Environments, 7–32. AGU Geophysical Monograph Series 164, Washington, D.C.

Kumar, G. (1997) Geology of Arunachal Pradesh: Bangalore. Geological Society of India, 217 p.

Lackey, J.S., Cecil, M.R., Windham, C.J., Frazer, R.E., Bindeman, I.N., and Gehrels, G.E. (2012) The Fine Gold Intrusive Suite: The roles of basement terranes and magma source development in the Early Cretaceous Sierra Nevada batholith. Geosphere, 8, 292–313.

Le Breton, N., and Thompson, A.B. (1988) Fluid-absent (dehydration) melting of biotite in metapelites in the early stages of crustal anatexis. Contributions to Mineralogy and Petrology, 99, 226–237.

LeFort, P. (1975) Himalayas, the collided range. Present knowledge of the continental arc. American Journal of Science, 275, 1–44.

——— (1996) Evolution of the Himalaya. In A. Yin and T. Harrison, Eds., The Tectonics of Asia, p. 95–106. Cambridge University Press, U.K.

LeFort, P., Vuney, M., Deniel, C., and France-Lanord, C. (1987) Crustal generation of the Himalayan leucogranites. Tectonophysics, 134, 39–57.

Luth, W.C., Jahns, R.H., and Tuttle, O.F. (1964) The granite system at pressures of 4 to 10 kilobars. Journal of Geophysical Research, 69, 759–773.

Maas, R., and McCulloch, M.T. (1991) The provenance of Archean clastic metasediments in the Narryer gneiss complex, Western Australia: Trace element geochemistry, Nd isotopes, and U-Pb ages from detrital zircons. Geochimica et Cosmochimica Acta, 55, 1915–1932.

Maas, R., Kinny, P.D., Williams, I., Froude, D.O., and Compston, W. (1992) The Earth's oldest known crust: A geochronological and geochemical study of 3900–4200 Ma old detrital zircons from Mt. Narryer and Jack Hills, Western Australia. Geochimica et Cosmochimica Acta, 56, 1281–1300.

Marchi, S., Bottke, W.F., Elkins-Tanton, L.T., Bierhaus, M., Wuennemann, K., Morbidelli, A., and Kring, D.A. (2014) Widespread mixing and burial of Earth's Hadean crust by asteroid impacts. Nature, 511, 578–582.

Massonne, H.-J., and Schreyer, W. (1987) Phengite geobarometry based on the limiting assemblage with K-feldspar, phlogopite, and quartz. Contributions to Mineralogy and Petrology, 96, 212–224.

Massonne H.-J., and Szpurka, Z. (1997) Thermodynamic properties of white micas on the basis of high-pressure experiments in the systems K2O-MgO-Al2O3-SiO2-H2O and K2O-FeO-Al2O3-SiO2-H2O. Lithos, 41, 229–250.

Menneken, M., Nemchin, A.A., Geisler, T., Pidgeon, R.T., and Wilde, S.A. (2007) Hadean diamonds in zircon from Jack Hills, Western Australia. Nature, 448, 917–920.

Mojzsis, S.J., Harrison, T.M., and Pidgeon, R.T. (2001) Oxygen-isotope evidence from ancient zircons for liquid water at the Earth's surface 4300 Myr ago. Nature, 409, 178–181.

O'Neil, J., Carlson, R.W., Francis, D., and Stevenson, R.K. (2008) Neodymium-142 evidence for Hadean mafic crust. Science, 321, 1828–1831.

O'Neill, C., and Debaille, V. (2014) The evolution of Hadean-Eoarchaean geodynamics. Earth and Planetary Science Letters, 406, 49–58.

Paces, J.B., and Miller, J.D. (1993) Precise U-Pb ages of Duluth Complex and related mafic intrusions, northeastern Minnesota: Geochronological insights to physical, petrogenetic, paleomagnetic, and tectonomagmatic processes associated with the 1.1 Ga Midcontinent Rift System. Journal of Geophysical Research, 98, 13997–14013.

Pan, G.T., Ding, J., Yao, D.S., and Wang, L.Q. (2004) Geological map of the Qinghai-Xizang (Tibet) Plateau and adjacent areas. Chengdu Cartographic Publishing House.

Peck, W.H., Valley, J.W., Wilde, S.A., and Graham, C.M. (2001) Oxygen isotope ratios and rare earth elements in 3.3 to 4.4 Ga zircons: Ion microprobe evidence for high δ18O continental crust and oceans in the Early Archean. Geochimica et Cosmochimica Acta, 65, 4215–4229.

Rasmussen, B., Fletcher, I.R., Muhling, J.R., Gregory, C.J., and Wilde, S.A. (2011) Metamorphic replacement of mineral inclusions in detrital zircon from Jack Hills, Australia: Implications for the Hadean Earth. Geology, 39, 1143–1146.

Rollinson, H. (2008) Ophiolitic trondhjemites: a possible analogue for Hadean felsic "crust." Terra Nova, 20, 364–369.

Ruppel, C., and Hodges, K.V. (1994) Pressure-temperature-time paths from two-dimensional thermal models: Prograde, retrograde and inverted metamorphism. Tectonics, 13, 17–44.

Shirey, S.B., Kamber, B.S., Whitehouse, M.J., Mueller, P.A., and Basu, A.R. (2008) A review of the isotopic and trace element evidence for mantle and crustal processes in the Hadean and Archean: Implications for the onset of plate tectonic subduction. Geological Society of America Special Papers, 440, 1–29.

Sizova, E., Gerya, T., Brown, M., and Perchuk, L.L. (2010) Subduction styles in the Precambrian: insight from numerical experiments. Lithos, 116, 209–229.

Solomon, S.C. (1980) Differentiation of crusts and cores of the terrestrial planets: Lessons for the early Earth? Precambrian Research, 10, 177–194.

Trail, D., Mojzsis, S.J., Harrison, T.M., Schmitt, A.K., Watson, E.B., and Young, E.D. (2007) Constraints on Hadean zircon protoliths from oxygen isotopes, REEs and Ti-thermometry. Geochemistry, Geophysics, Geosystems (G3), 8, Q06014, doi 10.1029/2006GC001449.

Turner, G., Harrison, T.M., Holland, G., Mojzsis, S.J., and Gilmour, J. (2004) Xenon from extinct 244Pu in ancient terrestrial zircons. Science, 306, 89–91.

Turner, G., Busfield, A., Crowther, S., Mojzsis, S.J., Harrison, T.M., and Gilmour, J. (2007) Pu-Xe, U-Xe, U-Pb chronology and isotope systematics of ancient

zircons from Western Australia. Earth and Planetary Science Letters, 261, 491–499.

Ushikubo, T., Kita, N.T., Cavosie, A.J., Wilde, S.A., Rudnick, R.L., and Valley, J.W. (2008) Lithium in Jack Hills zircons: Evidence for extensive weathering of Earth's earliest crust. Earth and Planetary Science Letters, 272, 666–676, doi: 10.1016/j.epsl.2008.05.032.

Valley, J.W. (2003) Oxygen isotopes in zircon. Reviews in Mineralogy and Geochemistry, 53, 343–385.

Velde, B. (1965) Phengite micas: Synthesis, stability, and natural occurrence. American Journal of Science, 263, 886–913.

——— (1967) Si^{+4} content of natural phengite. Contributions to Mineralogy and Petrology, 14, 250–258.

Vidal, P., Cocherie, A., and Le Fort, P. (1982) Geochemical investigations of the origin of the Manaslu leucogranite (Himalaya, Nepal). Geochimica et Cosmochimica Acta, 46, 2279–2292.

Ward, P.D., and Brownlee, D. (2000) Rare Earth: Why Complex Life is Uncommon in the Universe, 335 pp. Copernicus, New York.

Watson, E.B., and Harrison, T.M. (2005) Zircon thermometer reveals minimum melting conditions on earliest Earth. Science, 308, 841–844.

Wetherill, G.W. (1980) Formation of the terrestrial planets. Annual Reviews in Astronomy and Astrophysics, 18, 77–113.

White, R.W., Powell, R.W., and Holland, T.J.B. (2001) Calculation of partial melting equilibria in the system Na_2O-CaO-K_2O-FeO-MgO-Al_2O_3-SiO_2-H_2O (NCKFMASH). Journal of Metamorphic Geology, 19, 139–153.

Yin, A., and Harrison, T.M. (2000) Geologic evolution of the Himalayan-Tibetan Orogen. Annual Review of Earth and Planetary Sciences, 28, 211–280.

Yin, A., Dubey, C.S., Kelty, T.K., Webb, A.A.G., Harrison, T.M., Chou, C.Y., and Célérier, J. (2009) Geologic correlation of the Himalayan orogen and Indian craton: Part 2. Structural geology, geochronology, and tectonic evolution of the Eastern Himalaya. Geological Society of America Bulletin, 122, 360–395.

Zhang, H.F., Harris, N., Parrish, R., Kelley, S., Zhang, L., Rogers, N., Argles, T., and King, J. (2004) Causes and consequences of protracted melting of the mid-crust exposed in the North Himalayan Antiform. Earth and Planetary Science Letters, 228, 195–212.